A Current Hysteresis Control Strategy for Switched Reluctance Machine Based on Genetic Algorithms and Finite Elements Analysis ⋆

Israel R. Soares * **Khristian M. de Andrade Jr** * **Allan G. de Castro** ** **Bernardo P. de Alvarenga** * **Geyverson T. de Paula** *

* *Escola de Engenharia Elétrica, Mecânica e de Computação, Universidade Federal de Goiás (e-mail: isr321@hotmail.com, khristianjr11@gmail.com, bernardo_alvarenga@ufg.br, geyverson@ufg.br).*
** *Escola de Engenharia de São Carlos, Universidade de São Paulo (e-mail: allangregori@gmail.com).*

Abstract: Many applications require efficient, low torque ripple motors; therefore, using a switched reluctance motor (SRM) in these cases requires a control technique that takes it into account. This paper proposes a novel control strategy that uses optimal reference phase currents obtained by Genetic Algorithm (GA) that minimize torque ripple while maintaining the overall stator current. The Genetic Algorithm (GA) used a Finite Element Analysis (FEA) model to choose the ideal phase currents for a set of rotor positions and reference torques. That model took mutual inductances, cross-coupling effects, and saturation into account. Upon determination of the ideal phase currents to track, a current hysteresis control strategy was proposed to maintain a load torque of $2Nm$ at $300rpm$. To validate the proposed technique, a comparison with a Direct Instantaneous Torque Control (DITC) strategy was performed, proving which it maintains the machine efficiency and reduces torque ripple.

Keywords: switched reluctance motor; finite element analysis; optimization; mathematical modeling; genetic algorithm

1. INTRODUCTION

The Switched Reluctance Motor (SRM) stands out among the other electric motors due to its features, such as robustness, high starting torque, wide operating speed range, fault tolerance, and magnet-free structure (Bostanci et al., 2017). However, one of its main problems is the high torque ripple (Ma et al., 2016). The torque ripple is mainly due to its switching operation and double salient magnetic circuit, and it causes mechanical stresses, mechanical losses, and noise. Many applications demand smooth torque; hence reducing torque ripple is a typical and recurring state-of-the-art goal (Fang et al., 2021; Debouza et al., 2018; Tarvirdilu-Asl et al., 2019).

There are several different strategies mentioned in the literature to attain that goal. Some of them are focused on the choice/optimization of the inverter firing angles (Bae and Krishnan, 2000; Dowlatshahi et al., 2013; Lee et al., 2009; Choi et al., 2002; Kusumi et al., 2018; Gundogmus et al., 2020; Huang et al., 2020; Ma et al., 2016; de Paula et al., 2021), torque sharing functions (Dowlatshahi et al., 2013; Lee et al., 2009), and field-oriented control (FOC) (Husain et al., 2013, 2016; Sudhoff, 1993; Vilela et al., 2021). Despite their differences, they all have the same goal: to minimize torque ripple while maintaining efficiency.

2. MATHEMATICAL MODELING

2.1 Electromagnetic Torque

As mentioned, the SRM has a double salient magnetic circuit. This results in a phase inductance varying with rotor position, leading to an electromagnetic torque T_e proportional to its derivative, as described in (1).

$$T_e = \frac{1}{2}\sum_{j=1}^{N}\sum_{k=1}^{N}\frac{\partial L_{jk}}{\partial\theta} i_j\, i_k \tag{1}$$

In which N is the number of phases, θ is the rotor angular position, L_{jk} is the self-inductance if $j = k$ or the mutual inductance between j- and k-phases otherwise, and i_j and i_m are respectively the j- and k- phase currents.

Similarly, the inductance also varies with the electric load level due to the rotor and stator core saturation. This makes (1) difficult to evaluate analytically. Another method for computing electromagnetic torque using the Maxwell Stress Tensor and FEA is displayed in (2).

$$T_e = \frac{l_{stk}\, r^2}{\mu_0}\int_0^{2\pi} \boldsymbol{B_r} \times \boldsymbol{B_\theta}\, d\theta \tag{2}$$

where l_{stk} is the stack length, μ_0 is the free space permeability, r is the airgap middle radius, $\boldsymbol{B_r}$ is the radial flux

⋆ This work was supported by CNPq, FAPEG and Coordenação de Aperfeiçoamento de Pessoal de Nível Superior - Brasil (CAPES) - Finance Code 001.

density and $\boldsymbol{B_\theta}$ is the tangential one, both calculated in the airgap middle.

That method yields precise results, but consumes more computational resources, generally being used to generate T_e-i-θ lookup tables offline (Mikail et al., 2013).

2.2 Optimal Phase Currents Search Based on Genetic Algorithms to Mitigate the Torque Ripple

Genetic algorithms are often employed to develop high-quality solutions to optimization and search problems. In the present work, the GA's objective is to search for optimal currents that lead to torque ripple reduction and Maximum Torque Per Ampère (MTPA) operation. It was executed for a set of reference torques $T_{ref} \in [T_{min}, T_{max}]$ and discrete rotor positions $\theta_e \in [0, \pi/p]$, p being the number of pole pairs, totalizing half electric period.

For some specific reference torque T_{ref} and rotor position θ_e, the n-th individual $\boldsymbol{I_n}(T_{ref}, \theta_e)$ in a population of size P has the shape of (3).

$$\boldsymbol{I_n}(T_{ref}, \theta_e) = \langle i_{a,\,n},\, i_{b,\,n}, i_{c,\,n} \rangle \tag{3}$$

where $\boldsymbol{I_n}(T_{ref}, \theta_e) \in M$, M being the search space

$$M = \{\langle i_a,\, i_b, i_c \rangle \in R^3 \mid 0 \leq i_a,\, i_b,\, i_c \leq I_{\max}\}$$

in which $I_{\max}$ is the maximum current allowed by the windings.

Two functions were considered to compose the fitness function. The first one, $f_1(T_{ref}, \boldsymbol{I_n}, \theta_e) \in R$, considers the quadratic error between the desired reference torque T_{ref} and the one obtained with the current individual $T_e(\boldsymbol{I_n}(\theta_e), \theta_e)$, as in (4).

$$f_1(T_{ref}, \boldsymbol{I_n}, \theta_e) = [T_{ref} - T_e(\boldsymbol{I_n}, \theta_e)]^2 \tag{4}$$

The second one, $f_2(\boldsymbol{I_n}(\theta_e)) \in R$, minimizes the necessary current to meet the minimum f_1. For each rotor position, f_2 is calculated via (5).

$$f_2(\boldsymbol{I_n}) = i_{a,\,n}^2 + i_{b,\,n}^2 + i_{c,\,n}^2 \tag{5}$$

Finally, the fitness function $J(T_{ref}, \boldsymbol{I_n}, \theta_e)$ is written as (6), based on (4) and (5).

$$J(T_{ref}, \boldsymbol{I_n}, \theta_e) = \frac{1}{1 + \lambda f_1(T_{ref}, \boldsymbol{I_n}, \theta_e) + f_2(\boldsymbol{I_n})} \tag{6}$$

In which $\lambda \in R$ is a weight factor that controls the importance of f_1 over f_2.

The ideal current lookup table is obtained when J is maximized by GA over a set of reference torques in one half electric period. Depending on the size of T_{ref} and θ_e sets, it may lead to high memory consumption on implementation. To avoid that, it is possible to add a PI controller based on torque error to adjust the precision error generated by using a small set of reference torques.

Algorithm 1 summarizes the proposed search method for the optimal stator currents. It searches for the best values of i_a, i_b, and i_c in solution candidates as seen in (3)–(5). Other restrictions beyond the M space search limits are not considered.

GA parameters are described in Table 1.

Algorithm 1 Pseudo-code for the proposed GA approach

```
for each θ_e do
    Randomly Initialize a population of P individuals
    I_n(θ_e), with n ∈ 1, ··· P
    while stop criteria not met do
        Offspring ← Selected Individuals
        Do crossover and mutation operations in the
        offspring
        for each individual I_n(θ_e) in offspring do
            Compute T_e(I_n(θ_e), θ_e)
            Evaluate fitness via fitness function
            J(I_n(θ_e), θ_e)
        end for
        Sort out the offspring individuals by minimal
        fitness value
        Replace current population with offspring
    end while
    Store the fittest individual for the current θ_e that
    yields min(J(I_n(θ_e), θ_e), n = 1, ··· P) in the fi-
    nal population
end for
```

Table 1. GA Parameters

Parameter	Type/Description	Value
Selection Method	Tournament with 3 individuals participating in each tournament	–
Population Size	–	80
Mutation Rate	Gaussian	1%
Crossover Rate	Two-point	60%
1st stop criterion	Max. number of generations	30
2nd stop criterion	Average change in the fitness value	$\leq 10^3$
λ	Weight factor that controls the importance of f_1 over f_2	2×10^{-3}

3. DYNAMIC SIMULATION

The SRM under analysis has its main dimensions detailed in Table 2 whereas its cross-section is presented in Fig. 1. The machine parameters are presented in Table 3.

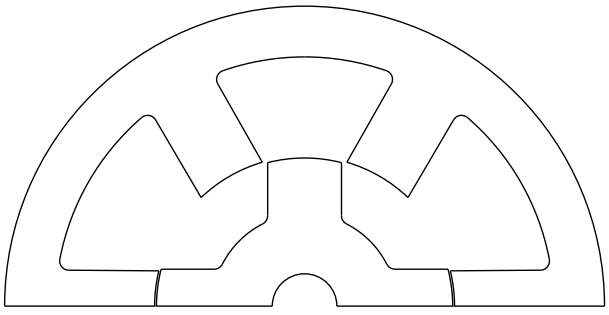

Figure 1. SRM cross-section.

To take into account the saturation and cross-coupling effects during the machine operation and improve liability of the dynamic simulation results aiming the torque ripple mitigation, the inductance and inductance derivative surfaces have been evaluated through Finite Element Analysis

Table 2. SRM Dimensions

Parameter	Value	Unit
Stator outer diameter	130	mm
Stator inner diameter	65	
Stator yoke	11	
Stator tooth height	21.5	
Stator tooth width	15.57	
Airgap	0.4	
Rotor outer diameter	64.2	
Rotor yoke	13	
Rotor tooth height	12	
Rotor tooth width	16	
Stack length	70	
Shaft diameter	14	
Turns per coil	190	–

Table 3. SRM Parameters

Parameters	Value	Unit
Stator poles	6	–
Rotor poles	4	
Phase resistance	3	Ω
Max. voltage	220	V
Rated power	375	W
Rated torque	2	Nm
Rated speed	1800	RPM
Moment of Inertia	4.2×10^{-3}	kg.m^2
Friction coefficient	3×10^{-5}	Nm.s

(FEA) and embedded in the dynamic simulation model as well as in the control scheme through look-up tables. The inductance and the inductance derivative for different electric/load conditions are shown in Fig. 2 and Fig. 3.

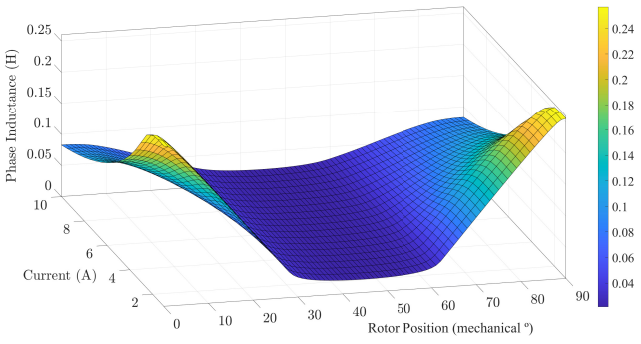

Figure 2. Phase inductance as a function of the position and load condition.

The proposed control strategy consists of an outer loop for speed control based on a PI controller that offers a reference torque. For each phase, the reference torque is converted to the reference currents using a look-up table provided by GA.

Additionally, a torque error PI controller is employed to generate Δi_{ref} to correct the GA obtained reference currents, which can be slightly imprecise due to discrepancies

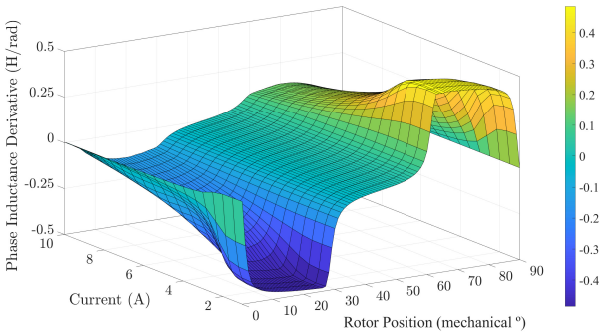

Figure 3. Phase inductance derivative as a function of the position and load condition.

between the machine construction and the machine FEA model.

Finally, the reference currents and the measured machine currents pass through a current hysteresis controller which generates the control signal to the active motor phase in the Asymmetric Half-Bridge (AHB) Converter. Figure 4 shows the proposed control scheme.

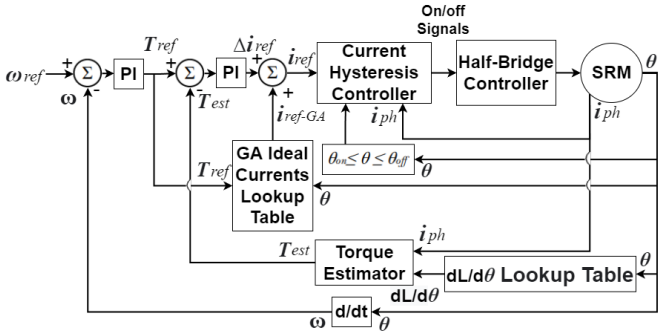

Figure 4. Proposed control strategy scheme

The speed error input PI, torque error input PI, and hysteresis controller parameters employed in the dynamic simulation are detailed in Table 4.

Table 4. Proposed Strategy Controller Parameters

Parameter	Value	Unit
DC bus voltage	220	V
PWM frequency	10	kHz
Speed PI k_p	0.02	–
Speed PI k_i	0.22	
Torque PI k_p	1.01	
Torque PI k_i	0.96	
Hysterisis band	0.1	A
Reference speed	300	RPM

To better showcase the proposed control strategy, a Direct Instantaneous Torque Control (DITC) strategy, as detailed in (Fang et al., 2021), was chosen. Table 5 details the controller parameters used. Its control scheme is depicted in Fig. 5.

The torque estimator block used in the two control strategies simulations is based on (1).

Table 5. DITC Strategy Controller Parameters

Parameter	Value	Unit
DC bus voltage	220	V
PWM frequency	10	kHz
Speed PI k_p	0.01	
Speed PI k_i	0.22	
Hysterisis band	0.1	A
Reference speed	300	RPM

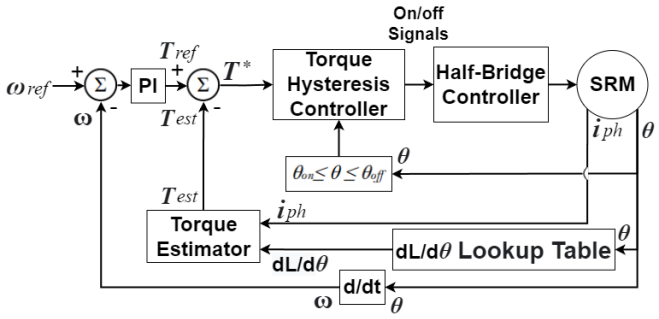

Figure 5. DITC strategy scheme

These simulations were started with a ramp load torque from $(0\ s, 0\ N.m)$ to $(0.1\ s, 2\ N.m)$, and after $0.1\ s$, $2\ N.m$ constant torque.

The θ_{on} and θ_{off} angles used in these control strategies are $52° \leq \theta \leq 85°$ for phase A, $82° \leq \theta \leq 90°$ and $0° \leq \theta \leq 25°$ for phase B, and $22° \leq \theta \leq 55°$ for phase C, comprehending one half electric period. These angles were obtained by the phase inductance surface shown in Fig. 2.

4. RESULTS AND DISCUSSION

The GA was used in conjunction with the FEA to account for any saturation or cross-coupling effects that may occur/exist. Figure 6 depicts the GA current waveform obtained for a 2 $N.m$ torque reference.

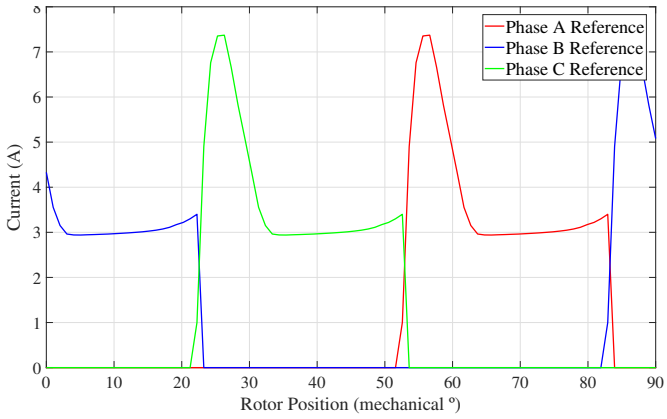

Figure 6. Current waveform obtained by GA for a 2 Nm torque reference.

The proposed control simulation performance is presented in Figs. 7-9. The DITC simulation performance is presented in Figs. 7, 8, and 10.

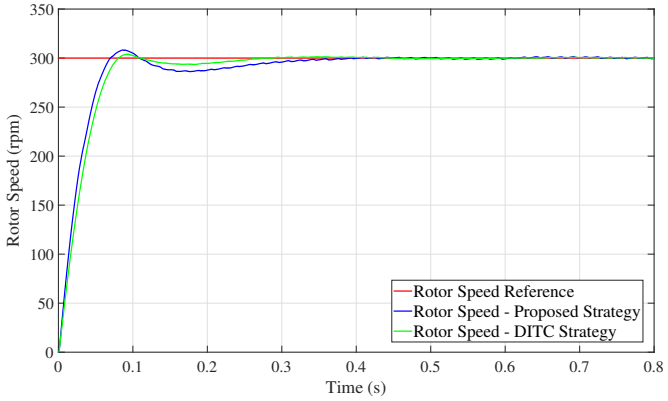

Figure 7. Rotor speed and rotor speed reference (rpm).

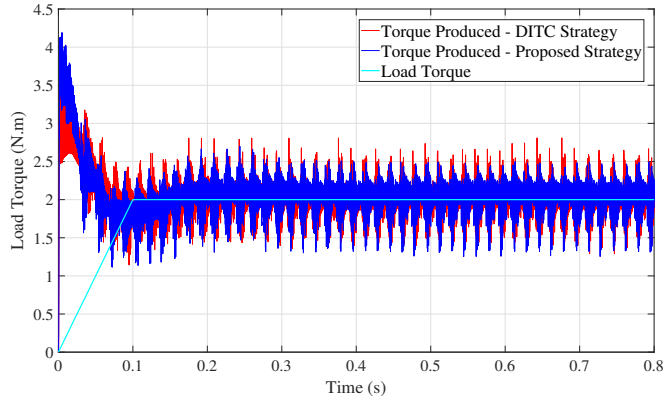

Figure 8. Load torque and torque in the proposed control strategy and DITC strategy

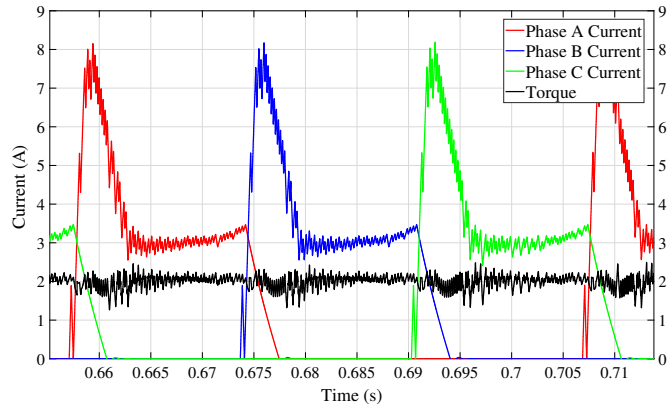

Figure 9. Phase Currents and the Electromagnetic torque for a constant reference torque - Proposed Strategy.

In Table 6, the torque ripple, torque ripple factor, and RMS current using the proposed control strategy and the DITC strategy are compared when the steady-state operation has been achieved. The torque ripple factor and the torque ripple are calculated by means of (7) and (8), respectively.

$$F_{\text{ripple}} = \left(\frac{T_{\text{ca}}}{T_{\text{avg}}}\right) \times 100\% \tag{7}$$

$$T_{\text{ripple}} = \left(\frac{T_{\text{max}} - T_{\text{min}}}{T_{\text{avg}}}\right) \times 100\% \tag{8}$$

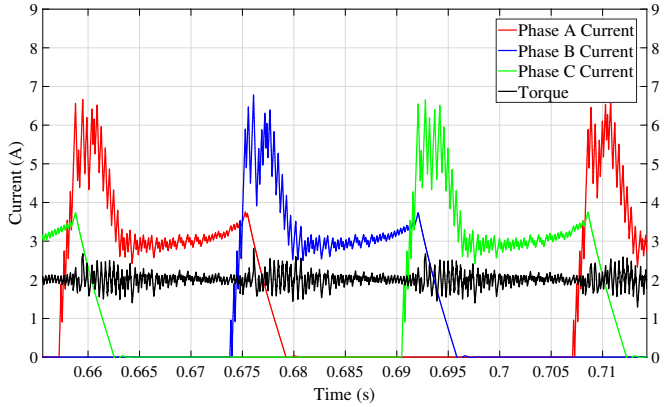

Figure 10. Phase Currents and the Electromagnetic torque for a constant reference torque - DITC Strategy.

where T_{avg} is the average torque; T_{min} and T_{max} are the minimum and maximum torque peak values, respectively; T_{ca} is the RMS of the resultant torque from the difference between the output torque and the average torque.

Table 6. Results

	DITC Strategy	Proposed Control Strategy	Unit
Reference torque	2		Nm
Reference speed	300		RPM
RMS current	2.27	2.40	A
Max. torque	2.81	2.50	
Min. torque	1.29	1.25	Nm
Avg. torque	2.0		
Torque ripple	75.95	62.38	%
Torque ripple factor	9.31	8.15	%
Avg. torque per Ampère	0.88	0.83	Nm/A

In 6, comparing the proposed control strategy with the DITC strategy, it is observed that the torque ripple is reduced by 17.86%, and the torque ripple factor is reduced by 12.45% when compared to the DITC strategy. The RMS current is increased by only 5.72%, which does not impact the overall machine efficiency. Therefore, the results show that the proposed control strategy has effectively diminished the torque ripple while maintaining the machine efficiency.

5. INDUCTIVE EFFECT AND THE GENETIC ALGORITHM IDEAL CURRENTS

Fig. 11 shows a comparison between a phase current and its reference. The main difference between them lies in the end of the waveform, where the GA obtained reference current is "ideally" turned off, whereas the actual current is still producing electromagnetic torque (opposing torque) due to the inductive effect of the phase winding, which is justified by (9).

$$\frac{\partial i_n}{\partial t} = \frac{1}{L_n}(V - i_n(\omega_r \frac{\partial L_n}{\partial \theta} + R)) \quad (9)$$

Where L_n (H) is the n-th phase inductance, i_n (A) is the n-th phase current, V (V) is the AHB converter's DC bus voltage, ω_r (rad/s) is the rotor speed and R (Ω) is the phase resistance.

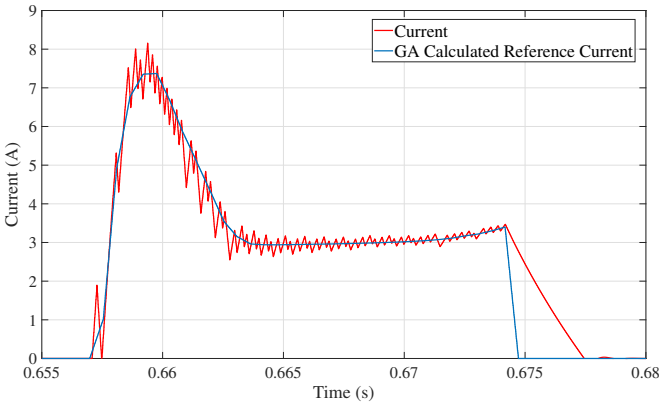

Figure 11. Comparison between one phase current and the reference current obtained by GA.

When a phase commutation occurs, a large current variation is required to extinguish the outgoing phase current to allow it to follow the reference current. However, at this time, the phase inductance is at its maximum, slowing the current fall. Other factors that may similarly contribute to it are high speed operation and low voltage on the AHB converter's DC bus. To operate at high speeds, it may be necessary to adjust the optimum GA currents in order to make the controller track it appropriately.

6. CONCLUSION

The proposed control strategy, which is based on the reference current obtained by a genetic algorithm approach and finite element analysis, is capable of reducing the torque ripple at 300 *rpm*. A comparison between that strategy and a DICT control strategy has shown that the torque ripple can be reduced by 17.86% and the torque ripple factor by 12.45% by implementing it. It was discussed the Inductive Effect that could impact the current track ability of the proposed control strategy. That effect was caused mainly by the high inductance of the outgoing phase at commutation period. In future works, experimental data will be considered.

7. ACKNOWLEDGEMENTS

This work was supported by CNPq, FAPEG and Coordenação de Aperfeiçoamento de Pessoal de Nível Superior - Brasil (CAPES) - Finance Code 001.

REFERENCES

Bae, H.K. and Krishnan, R. (2000). A novel approach to control of switched reluctance motors considering mutual inductance. In *2000 26th Annual Conference of the IEEE Industrial Electronics Society. IECON 2000. 2000 IEEE International Conference on Industrial Electronics, Control and Instrumentation. 21st Century Technologies*, volume 1, 369–374 vol.1. doi:10.1109/IECON.2000.973178.

Bostanci, E., Moallem, M., Parsapour, A., and Fahimi, B. (2017). Opportunities and challenges of switched reluctance motor drives for electric propulsion: A comparative study. *IEEE Transactions on Transportation Electrification*, 3(1), 58–75. doi:10.1109/TTE.2017.2649883.

Choi, C., Kim, S., Kim, Y., and Park, K. (2002). A new torque control method of a switched reluctance motor using a torque-sharing function. *IEEE Transactions on Magnetics*, 38(5), 3288–3290. doi:10.1109/TMAG.2002.802295.

de Paula, M.V., Barros, T.A.d.S., Moreira, H.S., Catata, E.O.H., Villalva, M.G., and Filho, E.R. (2021). A dahlin cruise control design method for switched reluctance motors with minimum torque ripple point tracking applied in electric vehicles. *IEEE Transactions on Transportation Electrification*, 7(2), 730–740. doi:10.1109/TTE.2020.3019997.

Debouza, M., Al-Durra, A., Hasanien, H.M., Leng, S., and Taha, W. (2018). Optimization of switched reluctance motor drive firing angles using grey wolf optimizer for torque ripples minimization. In *IECON 2018 - 44th Annual Conference of the IEEE Industrial Electronics Society*, 619–624. doi:10.1109/IECON.2018.8591473.

Dowlatshahi, M., Nejad, S.M.S., and Ahn, J.W. (2013). Torque ripple minimization of switched reluctance motor using modified torque sharing function. In *2013 21st Iranian Conference on Electrical Engineering (ICEE)*, 1–6. doi:10.1109/IranianCEE.2013.6599580.

Fang, G., Scalcon, F.P., Xiao, D., Vieira, R.P., Gründling, H.A., and Emadi, A. (2021). Advanced control of switched reluctance motors (srms): A review on current regulation, torque control and vibration suppression. *IEEE Open Journal of the Industrial Electronics Society*, 2, 280–301. doi:10.1109/OJIES.2021.3076807.

Gundogmus, O., Haque, M.E., Vadamodala, L., Bandarkar, A.W., Chowdhury, A., Sozer, Y., Venegas, F., and Colavincenzo, D. (2020). Current profile optimization method for simultaneous dc-link current ripple and acoustic noise minimization in switched reluctance machines. In *2020 IEEE Energy Conversion Congress and Exposition (ECCE)*, 5574–5579. doi:10.1109/ECCE44975.2020.9235609.

Huang, L., Zhu, Z.Q., Feng, J., Guo, S., Li, Y., and Shi, J.X. (2020). Novel current profile of switched reluctance machines for torque density enhancement in low-speed applications. *IEEE Transactions on Industrial Electronics*, 67(11), 9623–9634. doi:10.1109/TIE.2019.2952801.

Husain, T., Elrayyah, A., Sozer, Y., and Husain, I. (2013). Dq control of switched reluctance machines. In *2013 Twenty-Eighth Annual IEEE Applied Power Electronics Conference and Exposition (APEC)*, 1537–1544. doi:10.1109/APEC.2013.6520501.

Husain, T., Elrayyah, A., Sozer, Y., and Husain, I. (2016). Flux-weakening control of switched reluctance machines in rotating reference frame. *IEEE Transactions on Industry Applications*, 52(1), 267–277. doi:10.1109/TIA.2015.2469778.

Kusumi, T., Hara, T., Umetani, K., and Hiraki, E. (2018). Theoretical derivation of phase current profile for switched reluctance motors to suppress radial force ripple and torque ripple. In *2018 IEEE 27th International Symposium on Industrial Electronics (ISIE)*, 1037–1042. doi:10.1109/ISIE.2018.8433685.

Lee, D.H., Liang, J., Lee, Z.G., and Ahn, J.W. (2009). A simple nonlinear logical torque sharing function for low-torque ripple sr drive. *IEEE Transactions on Industrial Electronics*, 56(8), 3021–3028. doi:10.1109/TIE.2009.2024661.

Ma, C., Qu, L., Mitra, R., Pramod, P., and Islam, R. (2016). Vibration and torque ripple reduction of switched reluctance motors through current profile optimization. In *2016 IEEE Applied Power Electronics Conference and Exposition (APEC)*, 3279–3285. doi:10.1109/APEC.2016.7468336.

Mikail, R., Husain, I., Sozer, Y., Islam, M.S., and Sebastian, T. (2013). Torque-ripple minimization of switched reluctance machines through current profiling. *IEEE Transactions on Industry Applications*, 49(3), 1258–1267. doi:10.1109/TIA.2013.2252592.

Sudhoff, S. (1993). Multiple reference frame analysis of a multistack: variable-reluctance stepper motor. *IEEE Transactions on Energy Conversion*, 8(3), 418–424. doi:10.1109/60.257054.

Tarvirdilu-Asl, R., Nalakath, S., Bilgin, B., and Emadi, A. (2019). A finite control set model predictive torque control for switched reluctance motor drives with adaptive turn-off angle. In *IECON 2019 - 45th Annual Conference of the IEEE Industrial Electronics Society*, volume 1, 840–845. doi:10.1109/IECON.2019.8927841.

Vilela, W.M., de Andrade Jr, K.M., Santos, H.E., de Alvarenga, B.P., de Oliveira, E.S.L., and de Paula, G.T. (2021). Novel vector control approach for switched reluctance machines based on non-sinusoidal dq transform. *Journal of Control, Automation and Electrical Systems*, 33(1), 345–358. doi:10.1007/s40313-021-00810-0. URL `https://doi.org/10.1007/s40313-021-00810-0`.